Reflow Soldering-Resistant Solid-State 3D Micro-Supercapacitors Based on Ionogel Electrolyte for Powering the Internet of Things

B. Asbani, Botayna Bounor, K. Robert, C. Douard, L. Athouël, C. Lethien, J. Le Bideau, T. Brousse

Journal of The Electrochemical Society

OPEN ACCESS

Reflow Soldering-Resistant Solid-State 3D Micro-Supercapacitors Based on Ionogel Electrolyte for Powering the Internet of Things

To cite this article: B. Asbani *et al* 2020 *J. Electrochem. Soc.* **167** 100551

Journal of The Electrochemical Society, 2020 **167** 100551

Reflow Soldering-Resistant Solid-State 3D Micro-Supercapacitors Based on Ionogel Electrolyte for Powering the Internet of Things

B. Asbani,[1,2,3] B. Bounor,[1,2,3] K. Robert,[2,3] C. Douard,[1,3] L. Athouël,[1,3] C. Lethien,[2,3,z] J. Le Bideau,[1,3] and T. Brousse[1,3,*,z]

[1]*Université de Nantes, CNRS, Institut des Matériaux Jean Rouxel, IMN, F-44000 Nantes, France*
[2]*Institut d'Electronique, de Microélectronique et de Nanotechnologies, Université de Lille, CNRS, Centrale Lille, ISEN, Université de Valenciennes, UMR 8520—IEMN, F-59000 Lille, France*
[3]*Réseau sur le Stockage Electrochimique de l'Energie, CNRS FR 3459, 80039 Amiens Cedex, France*

The fabrication of all solid-state 3D micro-supercapacitor is challenging for powering connected and miniaturized emerging electronics devices in the frame of the future Internet of Things paradigm. Here we highlight the design of a specific solid electrolyte based on ethylmethylimidazolium bis(trifluoromethanesulfonate)imide confined within polyvinylidenefluoride which enables to meet the requirements of safety, easy packaging, and leakage free 3D micro-supercapacitors. This ionogel-based microdevice (2 mm × 2 mm footprint area) exhibits good cycling stability over 30 000 cycles with an areal energy density of 4.4 μWh.cm^{-2} and a power density of 3.8 mW.cm^{-2}. It can also sustain the high temperature reflow soldering process (~250 °C–5 min) without damage, which is performed to directly bond surface mounted miniaturized devices onto printed circuit boards. This strategy not only provides a reference for the design of high-performance 3D interdigitated micro-supercapacitors, but also paves the way to their further implementation in miniaturized electronic chips for Internet of Things applications.
 [DOI: 10.1149/1945-7111/ab9ccc]

Manuscript submitted March 25, 2020; revised manuscript received May 27, 2020. Published June 24, 2020.

All solid-state micro-supercapacitors (MSC)[1–4] are attractive miniaturized power sources that can bring energy autonomy and required power to smart and connected sensors for Internet of Things (IoT). Unfortunately, providing fully integrated on-chip energy storage miniaturized devices is challenging especially with regard to the compatibility of state of the art MSC vs the requirements of the microelectronic industry. Among all the desired properties to implement MSC in miniaturized electronic systems, high power and energy densities, long term cycling ability as well as leakage-free components are required. Recently, most of the efforts have been devoted to increase the energy and power densities of micro-supercapacitors using liquid electrolytes via the design of nanostructured electroactive materials such as carbide-derived carbon,[5] carbon onions,[6] conducting polymers[7] and transition metal oxides and nitrides.[8–10] Manganese dioxide has been proposed as a promising porous electrode material which exhibits high areal capacitance when deposited as a thin film.[11,12] This high areal capacitance can be largely attributed to pseudocapacitance, which arises when, in addition to double layer charging, fast reversible redox reactions occur at the surface of the porous electrode.[13] These redox reactions provide a capacitive-like signature which is the meaning of the term pseudocapacitive which noticeably differs from battery-type electrodes which exhibit the usual redox peaks depicted for faradaic processes.[13–15]

The development of thin-film manufacturing technologies can be achieved via a wide range of techniques such as electrochemical polymerization,[16] inkjet printing[17] and layer-by-layer assembly.[18] In spite of such improvements, new approaches to electrode design have been identified in order to increase energy and power densities. As a matter of fact, top down or bottom up fabrication methods are classically used to fabricate high aspect ratio three-dimensional (3D) current collectors providing enlarged surface compared to standard 2D designs[19–21] while keeping the same footprint area. Nevertheless, step conformal deposition techniques are required to deposit the electroactive material on such 3D scaffold. Thus, a significant improvement of the energy per footprint area has been demonstrated while keeping short ion diffusion paths and good electron harvesting pathways[22] to address the power issue. Moreover, the overall performance of a micro-supercapacitor not only depends on the electrode materials but also on the electrolyte. The design of high-performance MSC not only requires an electrolyte with high ionic conductivity and a wide electrochemical window, but also robust mechanical and stable thermal behaviors. All these conditions are rarely fulfilled in studies dedicated to MSC. On one hand, aqueous electrolytes limit device operation to about 1.23 V due to electrochemical water decomposition at higher cell voltages. Moreover, such aqueous electrolyte, even embedded in gel-type separator, is submitted to water evaporation which drastically decreases the performance upon ageing. Unfortunately, such behavior is rarely pointed out in the related studies, and some tricks are usually used to prevent/delay water evaporation but they are of no practical use. Indeed, it is quite difficult to prevent water evaporation from such gel-type electrolyte. Subsequently, water loss drastically lowers the ionic conductivity of the gel which in turn penalizes power and energy densities. On the other hand, ionic liquids (ILs) exhibit larger operational voltage windows. When used in MSC, cell voltage up to 2.5 V has been demonstrated.[23] Such a large voltage window as compared to aqueous electrolyte has a significant impact on the energy density of the device, as the energy stored is proportional to the square of the voltage window. Despite such fair ionic conductivity and broad electrochemical window, still the liquid state of ILs at operating temperature entails packaging issues due to liquid leakage problems. However, one of the main advantages of ILs is their zero vapor pressure which prevents fading of ionic conductivity and capacitance upon cycling. With respect to this last drawback, the development of ionogels[23–30] should fit packaging requirements by preventing the leakage of IL while maintaining wide electrochemical window, ionic conductivity and safety. Such ionogels, which are solid-like electrolytes, consist of an IL confined within a solid host matrix. They can maintain the electrochemical properties of the corresponding confined IL while preventing any leakage risk. Some studies have demonstrated good electrochemical performance of ionogel electrolytes when implemented in planar micro-supercapacitors fabricated via laser scribing of reduced graphene oxide.[31] However, the areal energy and power densities (energy and power per footprint area) are limited due to their planar configuration and

*Electrochemical Society Member.
[z]E-mail: christophe.lethien@univ-lille.fr; thierry.brousse@univ-nantes.fr

the low mass loading of the graphene based electrodes. Subsequently, three-dimensional designs could considerably enhance the MSC areal performance when combined with solid state ionogel electrolyte.

However, preventing the leakage is not the only requirement for solid-like electrolyte. It must also resist the reflow soldering, also designated as solder reflow process, which is a key process in the microelectronics industry. The reflow soldering aims at melting the solder and heating the adjoining contacts, while avoiding overheating and damaging the electronic components. At the end of the process, the surface mounted (miniaturized) devices (SMD) are bonded to the printed circuit board (PCB). This soldering technology requires electronic components to withstand a high soldering temperature, usually a peak temperature of 523 K (250 °C) for a short time, typically few tens of seconds. This process is compatible with lead-free solders which are required to meet the new environmental requirements. The resistance of the electrolyte towards degradation and vaporization during annealing processes such as reflow soldering is a crucial issue with respect to the integration of MSC in IoT miniaturized devices. However, literature data is very poorly documented about the resistance of MSC toward reflow soldering.[23,32,33] NEC TOKIN has been marketing the FC Series of carbon-based supercapacitors that feature a reflow surface mounting compatibility, i.e. a heat resistance capability of 260 °C.[32] Nevertheless, this necessitates increasing up to 50% the pressure applied to the dilute sulfuric acid solution and by strengthening the packaging. In such conditions, the device successfully sustains the reflow soldering with only small increase in ESR and small casing deformation, but the maximum operating temperature is limited to 85 °C. Despite these advantages, these electrochemical capacitors are not miniaturized and directly compete with commercially available bulk-type EDLCs for different purposes such as memory back up of car navigation systems, DVD players, etc. More recently, a 14 mF all-printed paper based MSC was designed using two stencil printed carbon electrodes and IL as electrolyte.[33] This microdevice (3.2 mm × 2.5 mm × 0.175 mm) was encapsulated using silicon glue which efficiently prevents IL leakage. The resulting MSC was heat treated 40 s at 255 °C thus simulating the reflow soldering, without significant deterioration of performance. Although this opens the way for IL-based MSC, the cycling performance was not highlighted in this study and should suffer from reactivity between the electrolyte and the glue, probably due to the presence of fluoride species. Moreover, the related miniaturized device is not an interdigitated one and does not appear as suitable for collective fabrication which is a main requirement related to microelectronic processes. The thickness of 100 μm classifies it as a thick solid state device as we already depicted in two different studies, thus being out of the scope of MSC.[34,35]

In a previous work, we have shown that an ionogel solid like electrolyte addresses the microelectronics technology requirements.[24] However, this ionogel was obtained by an acidic synthesis allowed by the electrode materials we used, assembled as a sandwich type EDLC, which in turn led to moderate capacitance, energy and power densities. Such acidic route is not compatible with many materials, among which manganese oxide. In another work, we have shown that a polymer-based ionogel obtained by an acidic-free route allowed to reach an efficient device, but needing several reactants.[30] In the present study, we propose the fabrication of all solid state 3D micro-supercapacitors based on 3D interdigitated MnO_2 electrodes and a more straightforward ionogel chemistry. In the present study, we propose the fabrication of all solid state 3D micro-supercapacitors based on 3D interdigitated MnO_2 electrodes and a specifically tailored ionogel chemistry. Such 3D design was previously reported by our team using aqueous electrolyte and IL.[19] which prevented any practical use of the microdevice due to electrolyte leakage and water evaporation. However, this previous work served to validate the concept of 3D micro-supercapacitors based on 3D interdigitated MnO_2 electrodes which we turn in the present study as a technological process fully compatible with semiconductor device manufacturing used in the microelectronics industry.

Experimental

Preparation of 3D symmetric MnO_2/MnO_2 MSC.—The fabrication of interdigitated 3D electrodes has already been reported elsewhere.[19] High aspect ratio vertically aligned silicon microtubes were prepared by micromachining a silicon wafer. The micro-tubes pattern was defined by a photolithography step on the silicon wafer. The silicon wafer was then etched selectively through the photoresist masks using a Deep Reactive Ion Etching process (DRIE, PlasmaPro Estrelas100 equipment). Then, a second step using a Bosh process, consisting of cycles alternating etching and passivation steps, was performed to generate the 3D silicon based scaffold. The third and fourth steps of this process were, respectively, the conformal deposition of layers of an insulating material and of a current collector, respectively. Atomic Layer Deposition (ALD) technology has been selected as the conformal deposition technique.[19] A 100 nm thick insulating layer (Al_2O_3) was first deposited by ALD to isolate each electrode. A 40 nm thick platinum layer (ALD) was further used as the current collector and the seed layer for MnO_2 electroplating deposition. After the conformal deposition of the platinum layer, a photolithography step combined with a dry etching step were used to define the 3D interdigitated current collectors. At this stage of the fabrication, the electroactive material could be deposited on the fabricated current collectors. Such 3D interdigitated platinum current collectors were electrochemically cleaned by running 40 voltammetry cycles in 0.1 M H_2SO_4 from −0.35 to 1.5 V vs Ag/AgCl at 50 $mV.s^{-1}$ scan rate. Then, the MnO_2 thin film was deposited on the 3D interdigitated electrodes by pulsed electrodeposition technique. Electrolytic Manganese Dioxide (EMD) can be grown from the direct electrolysis of an aqueous bath of manganese sulfate ($MnSO_4$) dissolved in sulfuric acid (H_2SO_4). In order to ensure a conformal coating of the MnO_2 pseudocapacitive thin film[19] on the 3D interdigitated current collectors, a voltage-controlled and pulsed deposition technique was chosen. The MnO_2 film deposition was performed from a 0.1M $MnSO_4$ in 0.1M H_2SO_4 electrolytic solution using the following procedure: a first step at 1.15 V vs Ag/AgCl for 0.1 s and second step at open circuit potential (OCP) for 0.5 s. The number of deposition pulses determines the thickness of the film: in our case, 1200 cycles were performed leading to a 430 nm-thick MnO_2 film which corresponds to about 4.7 $mg.cm^{-2}$ of footprint area. This fast deposition procedure enabled the deposition of a conformal and homogeneous MnO_2 thin film within a short period of time. The deposits exhibit good adhesion to the 3D platinum-coated current collector.

Preparation of ionogel and casting.—The ionogel electrolyte was synthesized using a non-aqueous sol–gel route by dissolving PVDF in DMF (Carlo Erba) at 15 wt% overnight at room temperature; then ethyl,methylimidazolium bis(trifluorosulfonyl)imide (EMIm TFSI) (Solvionic, 99.9%) was added to the solution. The ionogel contains 85% vol of EMIm TFSI. After homogenization of this solution, the mixture was poured into a Teflon mold. Concomitantly, the same mixture was casted on the 3D MSC as a thin film using 4 μl of the precursor solution for each 0.04 cm^2 microdevice. This volume has been determined according to the complete filling of the microstructured electrodes by the resulting ionogel and a full coverage of the interdigitated patterns. Adding more precursor solution only increases the thickness of the microdevice without altering neither improving its performance. Gelation was completed at room temperature over 5 d for the pellets used for ionic conductivity measurements, and over 2 d for the thin films used for device performance evaluation. Prior to each characterization, samples were dried at 60 °C under vacuum (0.5 mbar) for 18 h.

The reflow process was carried on solid MSCs that were already submitted to 1400 galvanostatic cycles for comparison purpose. This reflow was performed under air atmosphere at 523 K for 5 min.

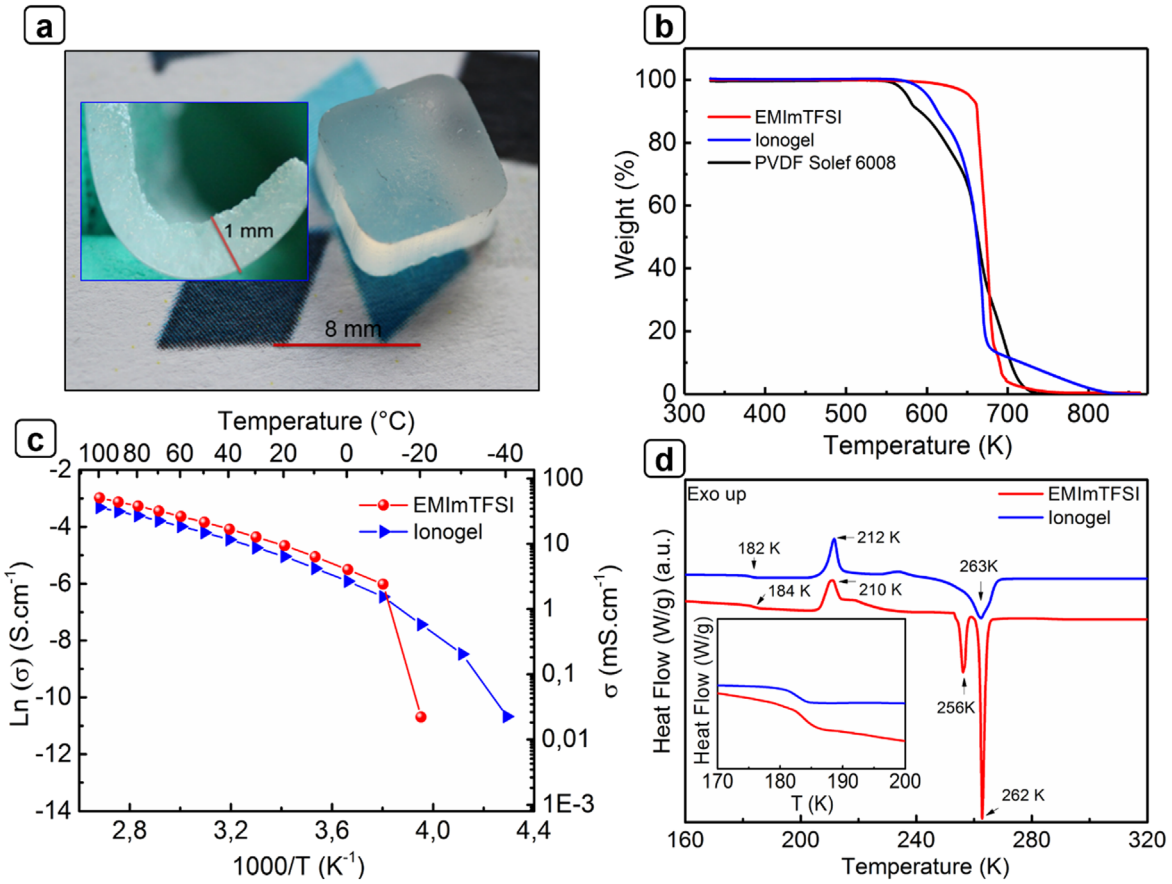

Figure 1. (a) Pictures of thick ionogel and of the 1 mm film (inset); (b) Thermogravimetric analysis (TGA) data of ionogel and comparison with the corresponding IL and PVDF; (c) ionic conductivities of the IL (EMIm TFSI) and of the corresponding ionogel at various temperatures; (d) DSC measurements comparing the IL and the corresponding ionogel.

Characterization.—The surface morphology was studied by scanning electron microscopy (SEM) performed on cross-sections of 3D interdigitated MSC using a Merlin Zeiss Field Effect microscope. Differential Scanning Calorimetry measurements (DSC) of the IL and of the ionogel were performed on a Netzsch STA449 F3 using hermetically sealed aluminum pans. The samples were quenched down to 150 K at 50 K min^{-1} followed measurements carried out during heating up to 333 K at 5 K min^{-1}. Thermogravimetric analyses (TGA) were carried out at a heating rate of 0.5 K min^{-1} under O_2 atmosphere using SETARAM Sensys Evo.

Electrochemical performance measurements.—The ionic conductivity of the ionogel was determined using electrochemical impedance spectroscopy (EIS) with a 50 mV amplitude within a 200 kHz–100 Hz frequency range on a Biologic VMP3 potentiostat/galvanostat equipment. The solid ionogel was inserted in a Swagelok cell between two stainless steel electrodes. This process was performed in a glove box under argon atmosphere. The measurement of the ionic conductivity of the IL also was performed in a Swagelok cell by using a Teflon ring spacer. The electrochemical properties of MnO_2 were evaluated by Cyclic voltammetry (CV), constant current galvanostatic charge and discharge cycling (GCPL), and electrochemical impedance spectroscopy (EIS) with a Biologic VMP3 potentiostat/galvanostat equipment. The performance of each MnO_2 electrode were first determined using a three-electrode configuration in 5 M $LiNO_3$ aqueous electrolyte, with a platinum wire as counter electrode and Ag/AgCl in saturated KCl solution as the reference electrode.

In the case of MnO_2 electrodes in IL-based electrolyte, performance were determined using two-electrodes and three-electrodes cell configurations in order to compare with the aqueous and ionogel electrolytes. The electrochemical properties of the MnO_2 electrodes in ionogel electrolyte were evaluated using two-electrodes cell configuration.

The specific capacitance (C, $mF.cm^{-2}$), energy density (E, $\mu Wh.cm^{-2}$), and power density (P, $mW.cm^{-2}$) were calculated according to the following equations:

$$C = \frac{\int Idt}{A\Delta V} \quad [1]$$

$$E = \frac{C(\Delta V)^2}{2} \quad [2]$$

$$P = 3600\frac{E}{\Delta t} \quad [3]$$

where I is the constant charge/discharge current (mA), Δt is the charge/discharge time, A represents the footprint area of the interdigitated MSC (0.04 cm^2) and ΔV is the cell voltage (V). The cycling tests were conducted using galvanostatic charge-discharge measurements with a constant current density of 1 $mA.cm^{-2}$.

Results and Discussion

Figures 1a–1b shows the pictures of bulk ionogel obtained after 5 d aging at room temperature. Crack-free transparent ionogel were obtained, either as films (1 mm) or as pellets. A 1 mm thick and ~1 cm long film of ionogel could be bent at 90° (Fig. 1a), and moreover did not show any leakage of liquid.

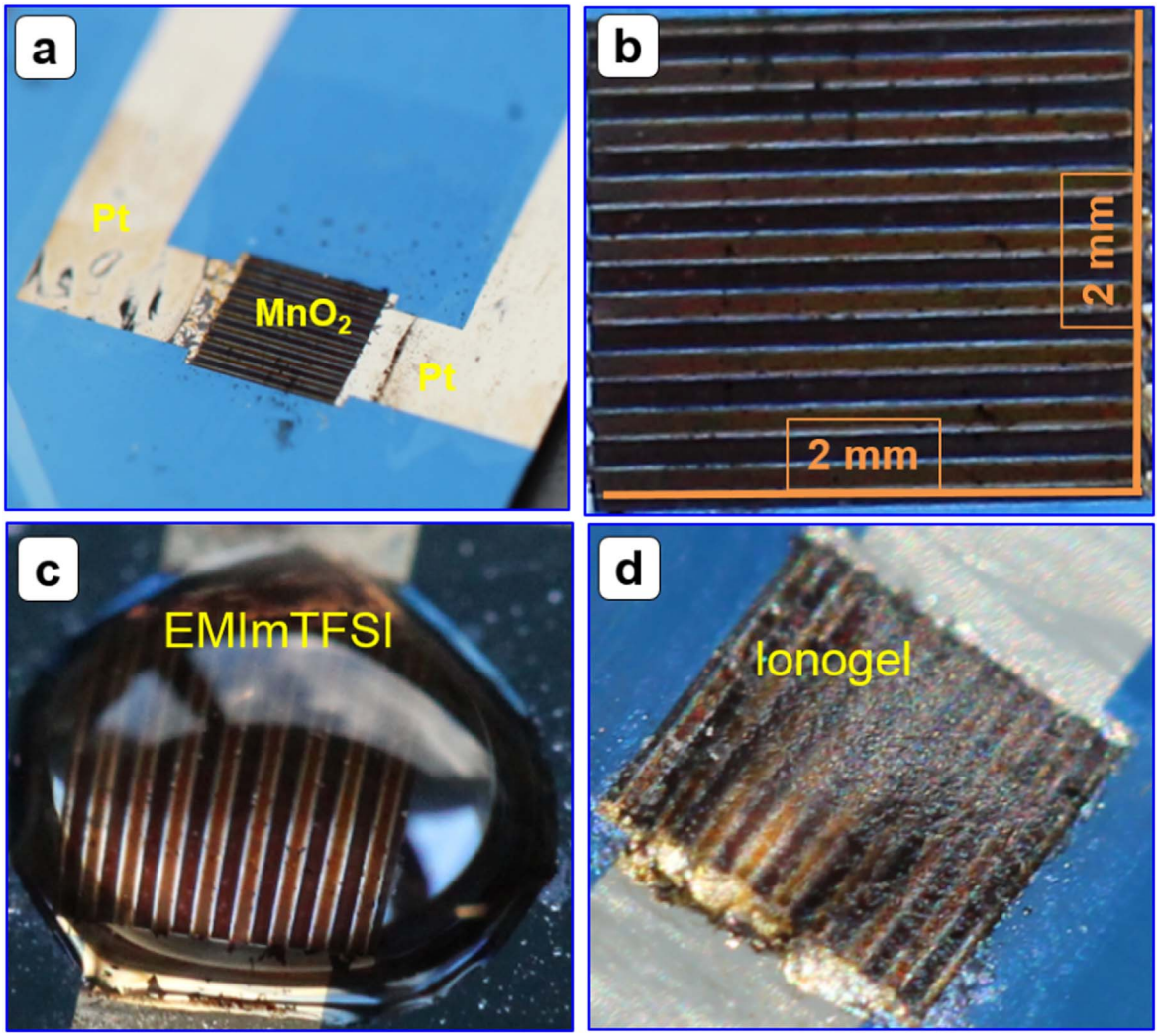

Figure 2. (a)–(b) Top View of 3D-interdigitated MSC with MnO_2 thin films as electrode material; (c) a drop of ionic liquid electrolyte deposited on the top of 3D interdigitated micro-supercapacitor (MSC); (d) ionogel on the top of the MnO_2-based MSC.

Thermogravimetric analysis TGA were carried out on the bulk ionogel to understand the role of confinement on the thermal stability of the IL. The TGA curves are depicted in Fig. 1b. The high thermal stability of the EMIm TFSI, of the PVDF and of the ionogel are clearly confirmed up to 550 K. Indeed, the decomposition of the IL starts at an onset temperature of 600 K which is 50 K higher than the starting decomposition temperature of PVDF. For the ionogel, the decomposition starts at 569 K. Since the reflow soldering temperature is close to 523 K, the ionogel may be advantageously implemented in the fabrication of MSC.

The ionic conductivity of the IL decreases drastically below −10 °C while it decreases only slowly for the ionogel Fig. 1c. Although the conductivity behavior at low temperatures is much better for the ionogel than for the non-confined IL, at temperatures above −10 °C both are very close. The good low temperature behavior of ionogel is obtained thanks to the quenching of the crystallization for the confined IL, allowing an increased ionicity and ions diffusion at the interface with the host network.[24]

As for prior studies, this observation is in good agreement with the DSC analysis (Fig. 1d) regarding the reduction of the enthalpy of crystallization peaks in the case of confined IL.

Figures 2a and 2b display the optical micrograph of a 3D interdigitated MSC before and after ionogel casting. The MSC consists in two interdigitated 3D electrodes composed of 8 digits ("fingers") (2 mm length and 100 μm width) per polarity. The spacing between two fingers is 20 μm while the footprint area of the MSC is 4 mm^2 (2 mm × 2 mm). Regarding the geometrical dimension of the 3D scaffold (diameter, spacing and etched depth), the area enhancement factor (AEF) is 30, meaning that 4 mm^2 footprint area leads to 120 mm^2 of available surface. A conformal deposition of nanostructured MnO_2 porous thin film onto the 3D conductive scaffold was performed by pulsed electroplating as observed on the images of the micro-supercapacitor (MnO_2-deposited electrode depicts a purple color), with a well-defined pattern and no short circuit between the interdigitated electrodes (Figs. 2a–2b). Prior to ionogel casting, a drop of IL was deposited on the top of the 3D ID MSC (Fig. 2c) and was easily spread which indicates a good wettability of the MnO_2 electrode by the EMIm TFSI IL. This will allowed comparing the performance of MSC either with non-confined IL or with confined IL (ionogel). Figure 2d illustrates the formation of the ionogel solid film after aging on the surface of 3D interdigitated (ID) MSC.

Figure 3 shows the top and cross-sections of the 3D MSC by SEM. Figure 3a depicts the top view of the 3D interdigitated platinum current collectors which consists of 16 fingers separated by an insulating layer. Each finger is based on an array of silicon microtubes (Figs. 3b–3c) coated with a conformal Pt thin film. Figures 3d–3f present similar views after MnO_2 deposition. It can be noticed that a conformal deposition of the MnO_2 layer is observed on the microtubes, thus validating the electrodeposition process. Figures 3g–3h also present similar views but after ionogel casting. From Fig. 3h it is possible to check that the ionogel completely

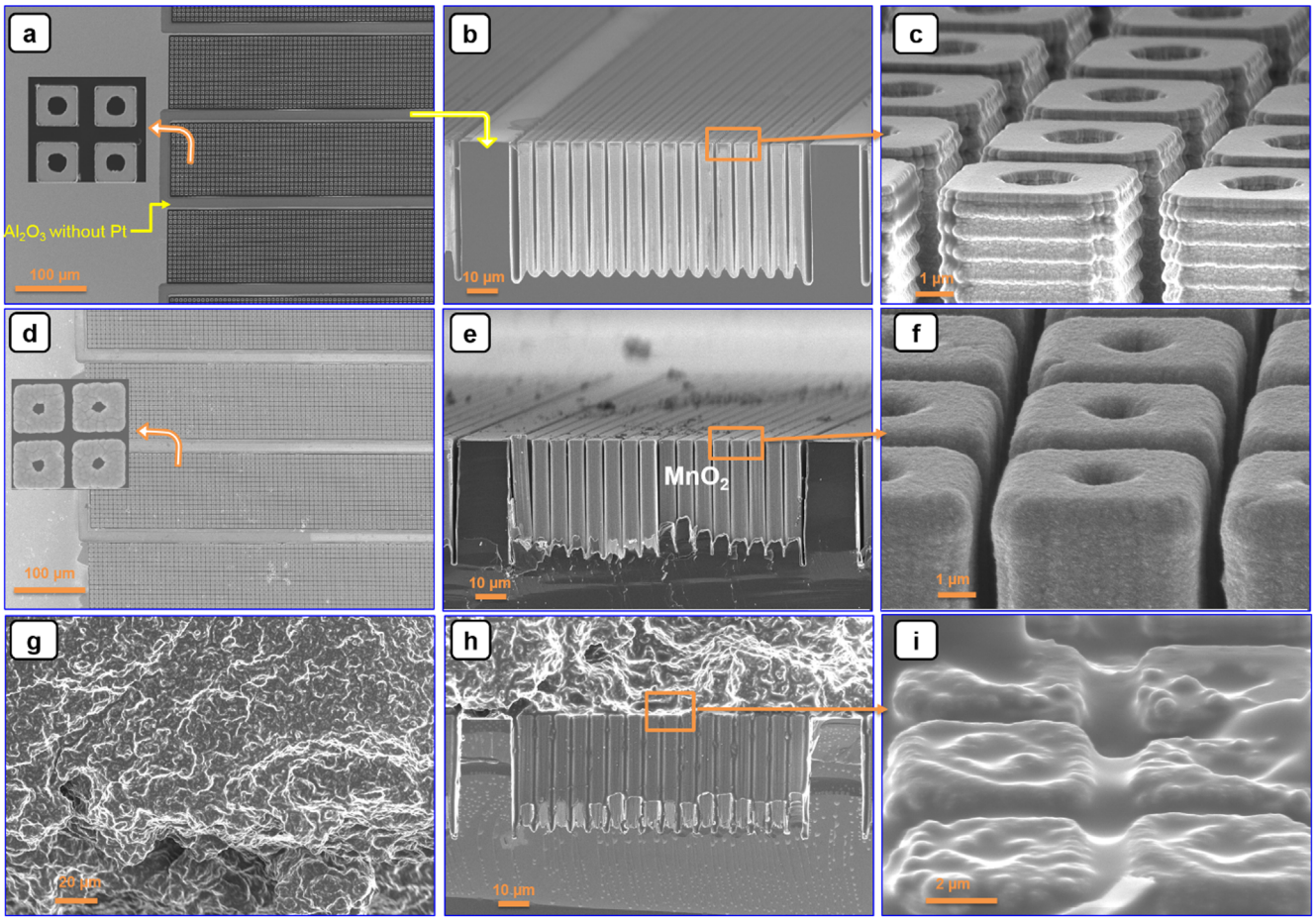

Figure 3. Scanning electron microscopy images showing the top, cross-section and tilted view of 3D interdigitated microstructures: (a)–(c) SEM images prior to electrodeposition of MnO_2; (d)–(f) SEM images of the conformal deposition of the MnO_2 thin film, prior to casting of the precursor of the ionogel; (g)–(j) SEM images of homogenous impregnation of 3D microstructures by the ionogel electrolyte (PVDF/EMIm TFSI—15/85%).

covers the spacing between the 3D microtubes, thus confirming the good wetting of the 3D scaffold by the sol precursor of the ionogel, prior to its polycondensation.

Electrochemical characterizations.—In order to evaluate the electrochemical performance of the MSC, the interdigitated electrodes design was used. Figures 4a–4d present the CV plots at different scan rates from 5 to 200 mVs^{-1} for a 3D MnO_2/MnO_2 interdigitated MSC in three different electrolytes, namely (i) 5 M $LiNO_3$ (aqueous electrolyte), (ii) EMIm TFSI (ionic liquid electrolyte) and (iii) EMIm TFSI/PVDF Ionogel (solid electrolyte). Whatever the electrolyte, the CV plots exhibit rectangular shape typically observed for pseudocapacitive MnO_2 based electrochemical capacitors.[13–15] It can be noted that the cell voltage of the symmetrical MnO_2 microdevice was kept below 1 V in order to avoid irreversible reduction of the negative electrode. Moreover, water molecules trapped in MnO2 nanostructure during pulse plating deposition can also be decomposed when the cell voltage exceeds 1.2 V. The CV plots still retain a quasi-rectangular shape even at high scan rates, thus suggesting that the 3D MSC can deliver high capacitance at high charge/discharge rates. Moving from aqueous to IL electrolyte (Figs. 4a and 4b) leads to a small decrease of the redox current (from 20 to 15 $mA.cm^{-2}$) while the capacitive-like behavior is maintained. Similar conclusions can be drawn when moving from IL (Figs. 4a and 4b) to ionogel solid electrolyte (Figs. 4c and 4d).

Figure 4e displays a plot of log (I) vs log (ν) from 20 to 200 mV s^{-1} for MnO_2 in different electrolyte. Assuming that the current is following a power-law relationship with the sweep rate:

$$I = a\nu^b \quad [4]$$

where I is the current (A), ν is the sweep rate ($mV.s^{-1}$), a and b are adjustable coefficients. The average b-value calculated is in between 0.83 and 0.6, calculated for the cathodic current at 1 V. Capacitive or pseudocapacitive processes should provide a b value close to 1 which is the case for aqueous $LiNO_3$ or IL based electrolytes. However, the confinement of IL in the polymer matrix clearly leads to a decrease in the b coefficient thus suggesting a diffusion limited process which could be due to the presence of more complex diffusion path in the solid electrolyte compared to the liquid ones.

The areal capacitances were extracted from the CV curves and plotted vs the sweep rate in Fig. 4f. Remarkably, the areal capacitance of the MSC in 5M $LiNO_3$ aqueous electrolyte is 118 $mF.cm^{-2}$ at 20 $mV.s^{-1}$ which confirms our previous reported results.[19] Regarding the interdigitated topology of the MSC, the surface capacitance of the MnO_2 thin film (0.43 μm-thick) is at least close to 0.48 $F.cm^{-2}$, i.e. four times higher than the capacitance of the full device. This value is two times higher than that of a 5 μm-thick carbide derived carbon electrode operated in 1M H_2SO_4 aqueous electrolyte.[3] The surface capacitance of the same MSC tested in EMIm TFSI is 78 $mF.cm^{-2}$, as depicted from the decrease of the current intensity observed on the CV plots. This lower value can be assigned to the lack of H^+ in the electrolyte. Indeed, H^+ species have been demonstrated to play a key role in charge storage on MnO_2 electrodes.[36] For the ionogel electrolyte, the specific capacitance is 36 $mF.cm^{-2}$ at 20 $mV.s^{-1}$.This decrease in capacitance compared to pure ionic liquid can be due to the wettability of

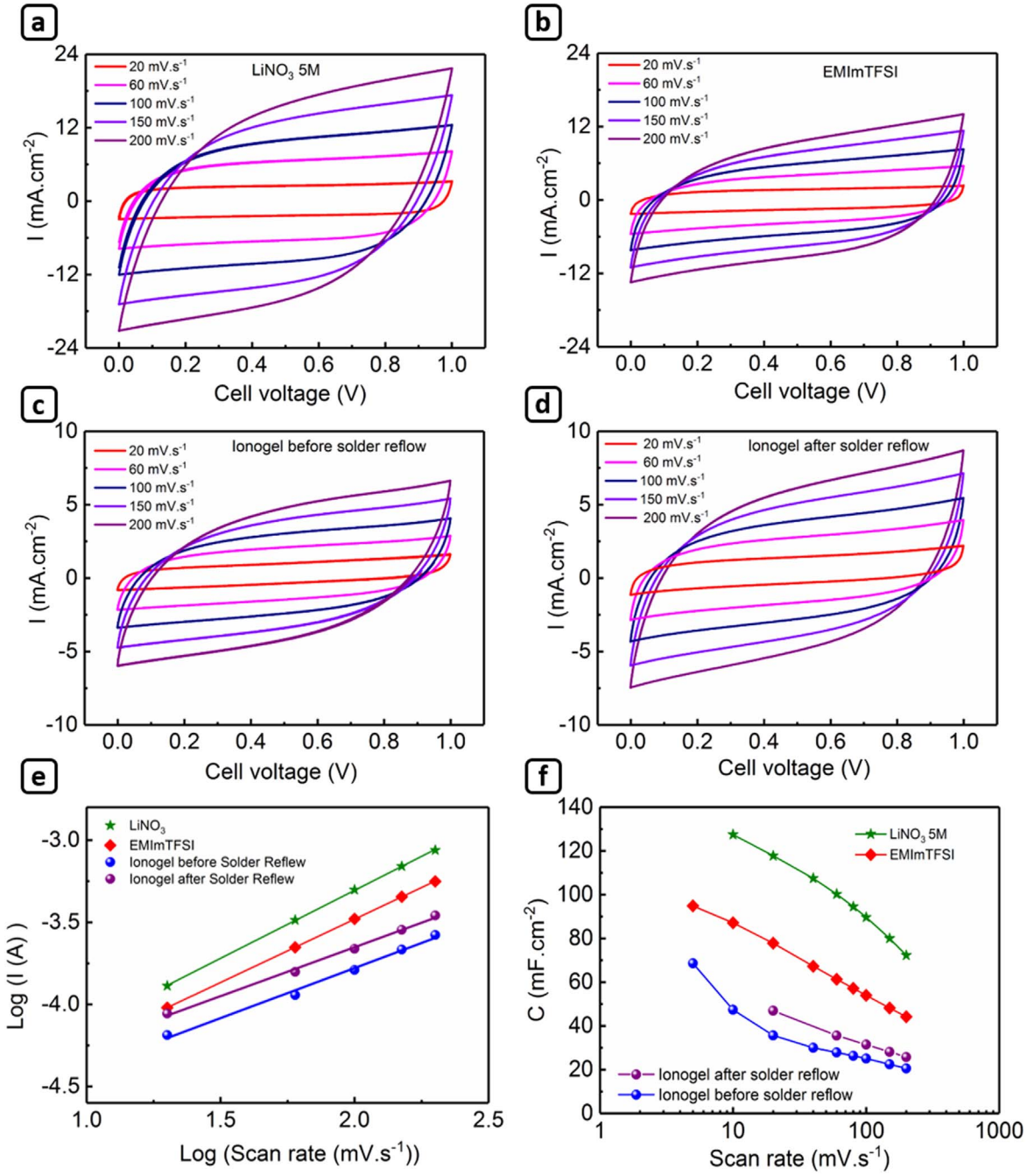

Figure 4. Electrochemical characterizations of a 3D interdigitated MSC with 4 mm^2 surface area; cyclic voltammograms at different sweep rates from 20 to 200 $mV.s^{-1}$ and tested in (a) 5M $LiNO_3$. (b) EMIm TFSI IL. (c) EMIm TFSI/PVDF ionogel electrolyte before reflow process (d) EMIm TFSI/PVDF ionogel electrolyte after reflow process (e) Current *vs* scan rate deduced from CV (f) Dependence of the surface capacitance *vs* scan rate in different electrolytes.

the MnO_2 electrode which is partially hindered by the polymer matrix. However, such capacitance value is 600 times higher than our previously reported silicon nanowires based solid state micro-supercapacitor, which was designed in a face to face geometry.[23]

Following these first electrochemical characterizations performed on the ionogel based device (Fig. 4c), the all solid state MSC was submitted to a reflow soldering process. Noticeably, it can be depicted from CV plots that the current is higher after the reflow soldering process (Fig. 4d). Consequently, the specific capacitance of the 3D MSC measured after the reflow soldering process increases up to 47 $mF.cm^{-2}$ at 20 $mV.cm^{-1}$. This 30% enhancement in the capacitance can be assigned to the annealing at 523 K for 5 min which improves the wetting of the IL onto the porous MnO_2 nanostructured material which in turn enhances the capacitance as previously observed for silicon nanowires.[23] This phenomenon could be due to the thermal dilatation, although small, of the IL which results in an increased IL amount at the surface of the ionogel upon heating.

In order to determine the areal energy and power densities of the 3D MnO_2/MnO_2 symmetric MSC, we carried out galvanostatic charge-discharge cycles at various current densities in different electrolytes. The charging and discharging parts of the plots are linear for lower current densities, illustrating triangular shape plots classically observed for electrochemical capacitors based on pseudocapacitive electrodes. The higher the current densities, the shorter the time constant (Figs. 5a–5c), the lower the surface capacitance. Similar GCPL plots with triangular shape profile are observed with solid state MSC before and after the reflow soldering process

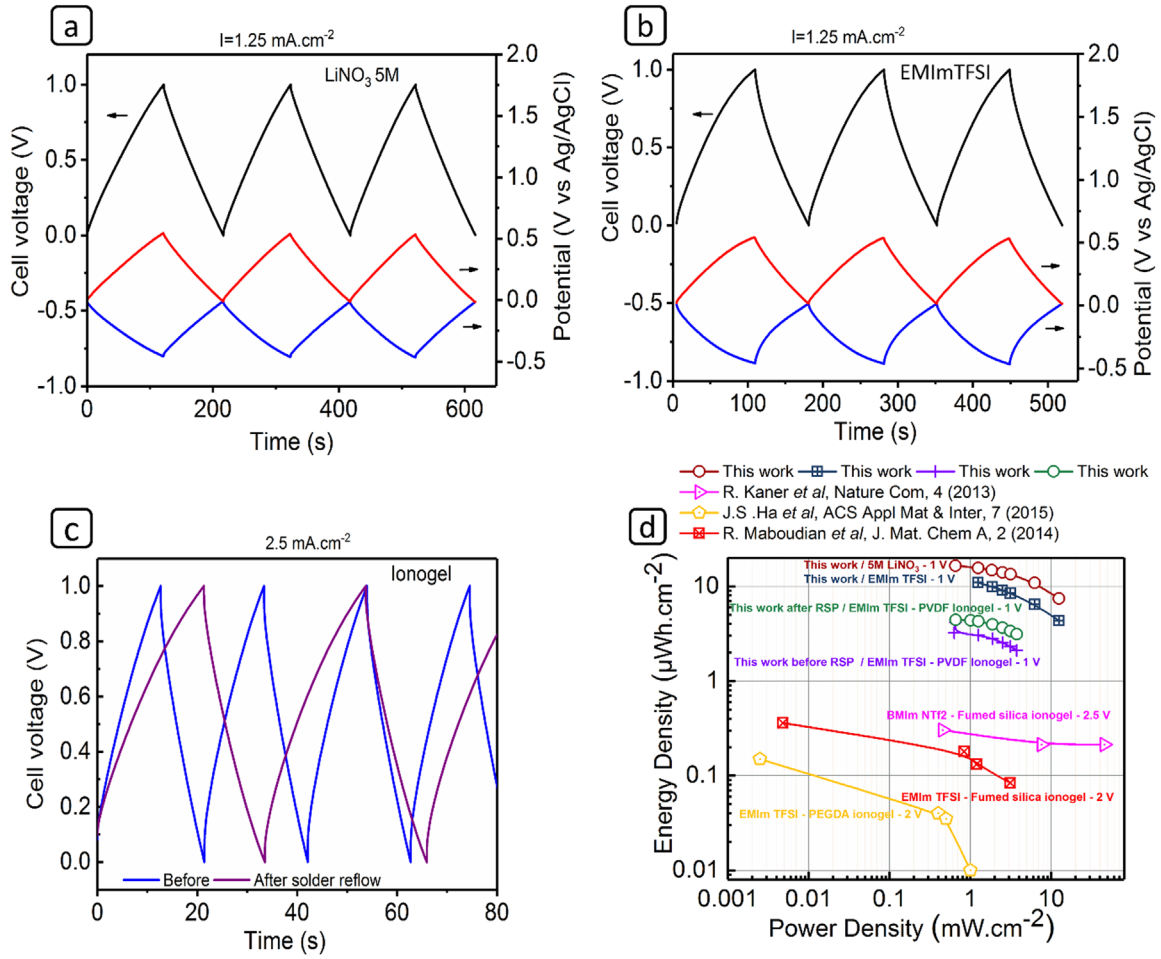

Figure 5. Electrochemical analyses of the MSC in different electrolytes. (a)–(c) Galvanostatic charge-discharge curves of the 3D MnO_2/MnO_2 MSC at various current densities tested in (a) 5M $LiNO_3$. (b) EMIm TFSI (Each electrode has been cycled under 0.5 V) (c) EMIm TFSI/PVDF ionogel electrolyte before reflow process and after solder reflow. (d) Ragone plot of all solid state micro-supercapacitors based on ionogels technologies as compared to the performance reached by our 3D MSC before and after solder reflow.

(Fig. 5c), confirming the pseudocapacitive behavior of the solid state MSC based on the EMIm TFSI/PVDF ionogel electrolyte.

The Ragone plot reporting the energy and power densities is depicted in Fig. 5d. At 1 $mW.cm^{-2}$ the areal energy density reaches 16.5 $\mu Wh.cm^{-2}$ in aqueous $LiNO_3$ electrolyte which is a similar value than reported in our previous work.[19] At the same power density, 10.9 $\mu Wh.cm^{-2}$ and 3.2 $\mu Wh.cm^{-2}$ are measured in EMIm TFSI and ionogel electrolytes, respectively. Such decrease of the performance could be attributed to the lower ionic conductivity of IL based electrolytes compared to aqueous $LiNO_3$.

After the reflow soldering process, the areal energy density is increased by 33%, reaching 4.4 $\mu Wh.cm^{-2}$ at the same power density. Whatever the power density, the general energy density of the 3D interdigitated MSC follows the same trend once the reflow soldering has taken place.

For a sake of clarity, we compare our results regarding the current state of the art micro-supercapacitors based on ionogels technology (Fig. 5d). In no case, MSC based on hydrogels "solid" electrolytes are taken into account because they suffer from water evaporation and cannot sustain reflow soldering. Kaner's group has published in 2013 the use of laser-scribed graphene as a very interesting carbon electrode (7.6 μm-thick) for electrical double layer micro-supercapacitor.[31] The areal energy density of the MSC reached 0.3 $\mu Wh.cm^{-2}$ while a high power density is maintained close to 50 $mW.cm^{-2}$. Those MSC exhibited a 2.5 V cell voltage. In 2014, R. Maboudian's group presented the used pyrolized photoresist as an efficient carbon electrode for MSC.[37] Combined with the ionogel technologies (EMIm TFSI/fumed silica ionogel), the fabricated MSC (1.2 μm-thick) was operated under 2 V and delivered a maximum areal energy density close to 0.36 $\mu Wh.cm^{-2}$. Recently, J.S. Ha et al. has published[38] in 2015 the use of photopaternable ionogel electrolyte (EMIm TFSI/PEGDA ionogel electrolyte) for micro-supercapacitor based on carbon multiwall nanotubes electrode (0.5 μm-thick). The technology was very attractive but again, the energy density stayed very low due to the use of planar carbon electrodes based on electroabsorption ion process. Within the frame of this study, we mix the fabrication of high performance 3D electrodes based on pseudocapacitive oxide materials and ionogel technology in order to fabricate all solid state 3D MSC at the wafer level for IoT applications.

Compared to our previous report on MSC able to sustain reflow soldering process, the areal energy density is 100 times higher than that of a MSC based on silicon nanowires.[23] The previous results were obtained on sandwich-type design which is not suitable for practical applications unlike our present device which uses interdigitated electrodes and can be implemented in any microelectronic based device. Moreover, the acidic chemistry route used for the ionogel in this previous work was not suitable for the present MnO_2 electrodes.

Long-term cycling is a key issue for electrochemical capacitors and for MSC dedicated to IoT applications with miniaturized sensors. MSC will be embedded as a part of the micro-power sources and requires performance stability after a large number of charge/discharge cycles.

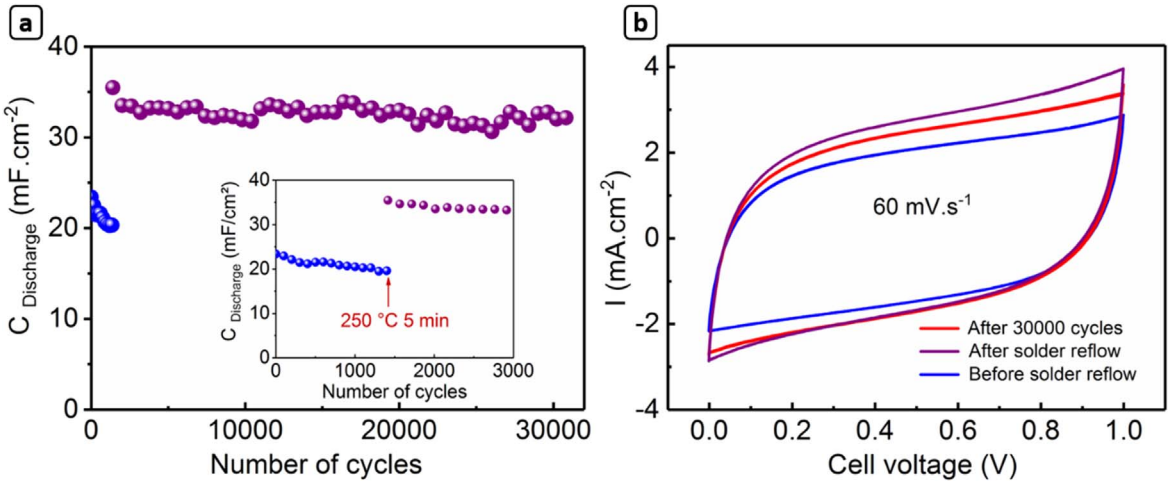

Figure 6. Long term cycling behavior of the 3D MSC based on EMiTFSI/PVDF ionogel electrolyte: (a) Areal capacitance vs the number of cycles measured at 1.75 mA.cm^{-2}; the inset shows the areal capacitance before and after heating at 523 K for 5 min under air; (b) CV measurement of the MSC before and after reflow process (blue and purple curves respectively) and the CV after 30000 GCPL cycles (red curve).

Such long-term cycling measurements have been performed on the all solid state 3D MnO_2/MnO_2 MSC based on EMIm TFSI/PVDF ionogel electrolyte. Figure 6a shows the areal discharge capacitance *vs* the number of cycles with a constant current density of 1.75 mA.cm^{-2} through more than 30 000 cycles. The GCDC plots show the typical charge/discharge triangular shape before and after the solder reflow process (Fig. 5c). The inset of Fig. 6a highlights the increase in capacitance after reflow process. To further evaluate the long term cycling properties of the all-solid state 3D micro-supercapacitor, the behavior of our all solid state MSC has been investigated before and after reflow process (523 K for 5 min) and after 30 000 galvanostatic charge/discharge cycles. CV experiments have been performed in order to compare the behavior of our MSC at different cycling stage as depicted in Fig. 6b. The electrochemical behavior of the fabricated solid state MSC is improved after the solder reflow process as depicted from the larger rectangular shape envelope than before with a 33% increase in capacitance as previously mentioned. A good cyclic stability is obtained for such 3D MSC based on reflow soldering resistant ionogel electrolyte which only shows a 3.8% capacitance fade upon 30 000 cycles. It can be pointed out that no differences were observed on the SEM images before and after long term cycling since electrochemical reactions take place at the electrode/electrolyte interface and thus cannot be simply observed by scanning electron microscopy. This good cycling stability goes together with the mechanical stability of the MSC thanks to the flexible properties of the ionogel electrolyte and the leakage free design. Indeed, further investigations will be performed on optimized microdevices using floating tests in order to determine the stability of the ionogel. Moreover, the improved behavior observed after the solder reflow seems to indicate a possible high temperature operation of the microdevice but this will be checked in a forthcoming study together with the potential detrimental use of low temperature.

Conclusions

The fabrication of an all solid state 3D interdigitated micro-supercapacitor (MSC) has been achieved, combining top down microfabrication technique, pulsed electroplating of porous nanostructured MnO_2 film as electrodes and ionogel drop casting. The ionogel electrolyte consists of 85% of EMIm TFSI ionic liquid confined in a PVDF host matrix. Such EMIm TFSI/PVDF ionogel electrolyte demonstrates high temperature thermal stability up to 569 K and retains the ionic conductivity of the ionic liquid component. This ionogel has been drop casted on a 4 mm^2 footprint area 3D interdigitated MnO_2/MnO_2 MSC. The resulting all solid state MSC is able to sustain reflow soldering process at 523 K classically used for surface mounted devices in electronic industry. Moreover, an improvement of the electrochemical performance has been observed after the annealing process. Such behavior is rarely reported in the literature. The ionogel-based MSC also exhibits good cycling stability over 30 000 cycles with an energy density of 4.4 μWh.cm^{-2} at a power density of 1 mW.cm^{-2} outperforming the current state of the art solid state microdevices. This strategy not only provides a solution for the design of high-performance 3D interdigitated MSC, but also paves the way to their further implementation in microelectronic devices for IoT applications.

Acknowledgments

This research benefitted from the financial support of the ANR within the DENSSCAPIO project (ANR-17-CE05-0015). The authors would also like to thank the ANR STORE-EX and the RS2E for their financial support. The RENATECH network receives our utmost gratitude. The authors declare no conflict of interest.

ORCID

L. Athouël https://orcid.org/0000-0001-9285-8925
C. Lethien https://orcid.org/0000-0001-8906-8308
J. Le Bideau https://orcid.org/0000-0003-3959-3694
T. Brousse https://orcid.org/0000-0002-1715-0377

References

1. C. Lethien, J. Le Bideau, and T. Brousse, *Energy Environ. Sci.*, **12**, 96 (2019).
2. N. A. Kyeremateng, T. Brousse, and D. Pech, *Nat. Nanotechnol.*, **12**, 7 (2016).
3. P. Huang et al., *Science*, **351**, 691 (2016).
4. D. He, A. J. Marsden, Z. Li, R. Zhao, W. Xue, and M. A. Bissett, *J. Electrochem. Soc.*, **165**, A3481 (2018).
5. J. Chmiola, C. Largeot, P.-L. Taberna, P. Simon, and Y. Gogotsi, *Science*, **328**, 480 (2010).
6. D. Pech, M. Brunet, H. Durou, P. Huang, V. Mochalin, Y. Gogotsi, P.-L. Taberna, and P. Simon, *Nat. Nanotechnol.*, **5**, 651 (2010).
7. G. Xiong, C. Meng, R. G. Reifenberger, P. P. Irazoqui, and T. S. Fisher, *Electroanalysis*, **26**, 30 (2014).
8. S. Wang, Z.-S. Wu, F. Zhou, X. Shi, S. Zheng, J. Qin, H. Xiao, C. Sun, and X. Bao, *npj 2D Mater. Appl.*, **2**, 7 (2018).
9. L. Coustan, A. Le Comte, T. Brousse, and F. Favier, *Electrochim. Acta*, **152**, 520 (2015).
10. K. Robert, C. Douard, A. Demortière, F. Blanchard, P. Roussel, T. Brousse, and C. Lethien, *Adv. Mater. Technol.*, **3**, 1800036 (2018).
11. E. Eustache, C. Douard, R. Retoux, C. Lethien, and T. Brousse, *Adv. Energy Mater.*, **5**, 1500680 (2015).
12. T. M. Dinh, F. Mesnilgrente, V. Conédéra, N. A. Kyeremateng, and D. Pech, *J. Electrochem. Soc.*, **162**, A2016 (2015).
13. T. Brousse, D. Bélanger, and J. W. Long, *J. Electrochem. Soc.*, **162**, A5185 (2015).
14. P. Simon, Y. Gogotsi, and B. Dunn, *Science*, **343**, 1210 (2014).
15. A. Balducci, D. Bélanger, T. Brousse, J. W. Long, and W. Sugimoto, *J. Electrochem. Soc.*, **164**, A1487 (2017).

16. J.-H. Sung, S.-J. Kim, S.-H. Jeong, E.-H. Kim, and K.-H. Lee, *J. Power Sources*, **162**, 1467 (2006).
17. D. Pech, M. Brunet, P.-L. Taberna, P. Simon, N. Fabre, F. Mesnilgrente, V. Conédéra, and H. Durou, *J. Power Sources*, **195**, 1266 (2010).
18. M. Beidaghi and C. Wang, *Adv. Funct. Mater.*, **22**, 4501 (2012).
19. E. Eustache, C. Douard, A. Demortière, V. D. Andrade, M. Brachet, J. Le Bideau, T. Brousse, and C. Lethien, *Adv. Mater. Technol.*, **2**, 1700126 (2017).
20. M. Ahmed, B. Wang, B. Gupta, J. J. Boeckl, N. Motta, and F. Iacopi, *J. Electrochem. Soc.*, **164**, A638 (2017).
21. N. Sun, X. Ma, Y. Su, P. Jiang, Y. Zou, and D. Zhou, *J. Electrochem. Soc.*, **166**, H802 (2019).
22. Y. Zargouni, S. Deheryan, A. Radisic, K. Alouani, and P. M. Vereecken, *Nanomater. Basel Switz.*, **7**, 126 (2017).
23. M. Brachet, D. Gaboriau, P. Gentile, S. Fantini, G. Bidan, S. Sadki, T. Brousse, and J. Le Bideau, *J. Mater. Chem. A.*, **4**, 11835 (2016).
24. A. Guyomard-Lack, P.-E. Delannoy, N. Dupré, C. V. Cerclier, B. Humbert, and J. Le Bideau, *Phys. Chem. Chem. Phys.*, **16**, 23639 (2014).
25. A. Guyomard-Lack, J. Abusleme, P. Soudan, B. Lestriez, D. Guyomard, and J. Le Bideau, *Adv. Energy Mater.*, **4**, 1301570 (2014).
26. M.-A. Néouze, J. Le Bideau, P. Gaveau, S. Bellayer, and A. Vioux, *Chem. Mater.*, **18**, 3931 (2006).
27. S. Mitra, C. Cerclier, Q. Berrod, F. Ferdeghini, R. De Oliveira-Silva, P. Judeinstein, J. Le Bideau, and J.-M. Zanotti, *Entropy.*, **19**, 140 (2017).
28. L. Nègre, B. Daffos, P. L. Taberna, and P. Simon, *J. Electrochem. Soc.*, **162**, A5037 (2015).
29. S. Song, S. Yang, F. Zheng, K. Zeng, H. M. Duong, S. V. Savilov, S. M. Aldoshin, N. Hu, and L. Lu, *J. Electrochem. Soc.*, **163**, A2887 (2016).
30. D. Aidoud, D. Guy-Buissou, D. Guyomard, B. Lestriez, and J. Le Bideau, *J. Electrochem. Soc.*, **165**, A3179 (2018).
31. M. F. El-Kady and R. B. Kaner, *Nat. Commun.*, **4**, 1475 (2013).
32. O. Keiichi, T. Kazuhiro, O. Keisuke, Y. Kohei, and M. TA Shinji, *NEC Tech. J.*, **4**, 81 (2009).
33. Y. Wang, W. Lai, Z. Jiang, and C. Yang, *IEEE Trans. Dielectr. Electr. Insul.*, **24**, 676 (2017).
34. M. Brachet, T. Brousse, and J. Le Bideau, *ECS Electrochem. Lett.*, **3**, A112 (2014).
35. B. Asbani, C. Douard, T. Brousse, and J. Le Bideau, *Energy Storage Mater.*, **21**, 439 (2019).
36. M. Toupin, T. Brousse, and D. Bélanger, *Chem. Mater.*, **16**, 3184 (2004).
37. S. Wang, B. Hsia, C. Carraro, and R. Maboudian, *J. Mater. Chem. A.*, **2**, 7997 (2014).
38. D. Kim, G. Lee, D. Kim, and J. S. Ha, "Air-stable, high-performance." *ACS Appl. Mater. Interfaces*, **7**, 4608 (2015).